Sensors and Actuators A 163 (2010) 311–314

Contents lists available at ScienceDirect

Sensors and Actuators A: Physical

journal homepage: www.elsevier.com/locate/sna

Short communication

# A two-liquid electroosmotic pump using low applied voltage and power

Shawn Litster[1], Matthew E. Suss, Juan G. Santiago*

*Department of Mechanical Engineering, Stanford University, Stanford, CA 94305-3030, USA*

ARTICLE INFO

*Article history:*
Received 5 January 2010
Received in revised form 24 June 2010
Accepted 13 July 2010
Available online 18 July 2010

*Keywords:*
Micropump
Electroosmotic pump
Electrokinetic pump
Flexible membrane pump
Drug delivery
Concentration polarization

ABSTRACT

We report the development and experimental analysis of a two-liquid electroosmotic (EO) pump. The pump uses a collapsible and impermeable membrane to separate the liquid delivered from a working electrolyte solution optimized for EO pumping. To achieve high pressures at low voltages, we use a porous glass substrate with 450 nm mean diameter pores and a 1 mM sodium borate electrolyte. Results show that the membranes add negligible pressure load and that the pump can deliver adequately stable flow rates after an initial transient period. At flow rates and pressures suitable for drug delivery (order 10 μl/min and a few kPa), the pump requires an applied voltage and power of less than 3 V and 75 μW, respectively. Based on the relative scaling of flow rate, current, and time, we hypothesize that distinct initial transients in flow rate are attributable to concentration polarization and its effects on the spatiotemporal ionic strength of the working fluid.



## 1. Introduction

Electroosmotic (EO) pumps utilizing porous glass substrates are well suited for a variety of micropump applications as they are compact, use low power, and have no moving parts [1–3]. EO pumps pump bulk liquid upon application of an electric field. Flow and pressure are a result of ion drag forces generated by mobile ions of electric double layers (EDL), which form at the solid-liquid interface. Porous glass substrates with small characteristic pore diameters provide high surface-to-volume ratio structures and high pressure per applied potential [3].

Several experimental studies of EO pumps have utilized applied voltages of over 1 kV for pumping [4–7], and electroosmotic pumps are often associated with the requirement of high-applied potentials [8,9]. However, such working voltages can be avoided with careful pump design. Pump pressure capacity scales as $fV_{\text{eff}}/a^2$, where $V_{\text{eff}}$ is the potential across the pump substrate and $a$ is the substrate mean pore radius. $f$ is an integral factor accounting for the finite EDL effects which approaches unity for relatively large pores, but decreases rapidly as pore diameter decreases and approaches the EDL length scale [2]. Tuning EO pumps to particular applications therefore requires careful choices of electrolyte chemistry, pore diameter, and pump area. As we shall see below, order 10 μl/min flow rates and a few kPa pressure capacities can be realized with just a few applied volts.

EO pumps are typically implemented in a "direct pumping" fashion in which the liquid delivered is also pumped through the porous substrate. This approach limits the applicability of EO pumping as the chemistry of the delivered stream can vary widely. As discussed by Yao and Santiago [2], low pH and high ionic concentration significantly reduces zeta potential and EO pump performance when using porous glass substrates. The working solution should also feature sufficient buffering capacity in order to maintain a relatively constant pH.

EO pumps with pumping performance independent of delivered fluid properties have been achieved with two-liquid design approaches. Such designs use a liquid optimized for EO pumping (hereafter referred to as the working electrolyte solution) to displace a secondary liquid (e.g., a drug). Glawdel et al. [10] achieved two-liquid EO pumping by separating the working and secondary liquids by oil (an immiscible fluid). Brask et al. [11] proposed a design using viscous drag exerted by the working fluid onto a secondary fluid in direct contact. Uhlig et al. [12] proposed the idea of using a collapsible bellows-like structure pressurized by a working electrolyte solution to displace a secondary liquid. The use of collapsible structures seems a promising technique, requiring less complexity than viscous drag designs and allowing for long-term and orientation-independent pumping. In early, preliminary work, Kim et al. [13] and Litster et al. [14] presented work towards EO pumps which incorporate collapsible membranes. In this work, we present the design, fabrication and characterization of a two-liquid pump employing collapsible membranes and a porous glass substrate with sub-micron pores for high pressure per

* Corresponding author at: 440 Escondido Mall, Bldg 530, rm 224, Stanford, CA 94305, USA. Tel.: +1 650 723 5689; fax: +1 650 723 7657.
*E-mail address:* juan.santiago@stanford.edu (J.G. Santiago).
[1] Department of Mechanical Engineering, Carnegie Mellon University, 5000 Forbes Ave., Pittsburgh, PA 15213, USA.

0924-4247/$ – see front matter © 2010 Elsevier B.V. All rights reserved.
doi:10.1016/j.sna.2010.07.008

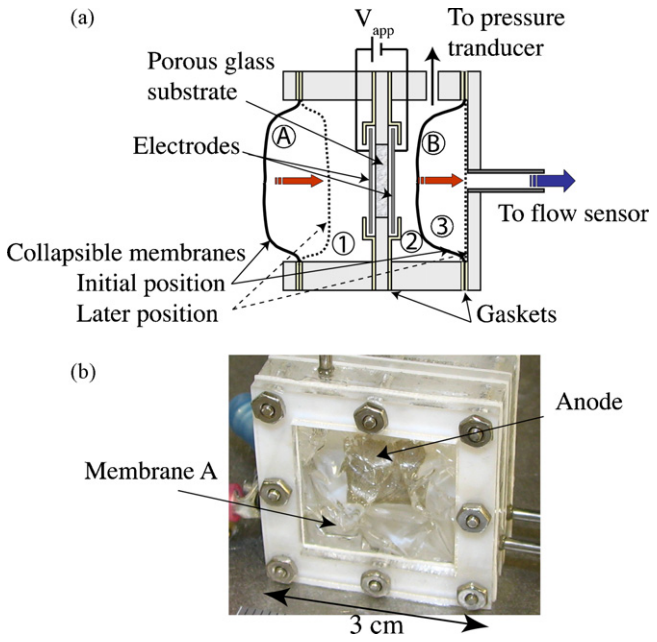


**Fig. 1.** (a) A schematic of the two-liquid EO pump. The working electrolyte is pumped from the anode reservoir (reservoir 1) to the cathode reservoir (reservoir 2) by electroosmosis. Membrane B displacement drives the secondary fluid in reservoir 3 through the outlet. The collapsible membrane A ensures that a negative pressure does not develop in the sealed anode reservoir. The initial position of the membranes and a later position are shown as solid and dashed lines respectively. (b) View of the two-liquid EO pump used from the anode side.

applied potential. We demonstrate that two-liquid pumping can be achieved at applied voltage and power of less than 3 V and 75 μW, respectively, while using low-cost plastic membranes.

## 2. Experimental

Fig. 1a presents a schematic of the pump architecture. The working electrolyte solution is initially contained in the anode reservoir (reservoir 1), which is bounded by a collapsible membrane (membrane A) and the porous substrate. The working electrolyte is then pumped into the initially collapsed membrane B, which forms a boundary of the cathode reservoir (reservoir 2). During pumping, membrane B expands within the otherwise rigid reservoir 3, thus driving the secondary fluid through the outlet. Membrane A prevents negative pressure from developing in the anode reservoir.

We fabricated the two-fluid pump as shown in Fig. 1b. EO pumping was generated using a square 1 $cm^2$, 2 mm thick porous glass substrate composed of silica and borosilcate particles (EoPlex Technologies, Redwood City, CA), with a 450 nm median pore diameter. We used solid platinum mesh electrodes (Goodfellow Cambridge Limited, UK) with 0.06 mm diameter wires and center-to-center spacings of 0.25 mm. Electrodes were placed against the substrate surface. The collapsible membranes were laser ablated from polyvinylidene chloride film to $39 \times 39\,mm^2$ (Saran Wrap, SC Johnson, Racine, WI). We selected this membrane material for its minimal resistance to deformation and folding, and adequate chemical resistance.

For all experiments, we use 1 mM ($Na^+$ concentration) borate buffer (J. T. Baker, Phillipsburg, NJ) as the working electrolyte. This buffer is well suited to EO pumping because of its high pH, buffering capacity, and low conductivity at 1 mM [3]. The buffer solution had a conductivity of 80 μS/cm and a pH of 9.3 (Corning Pinnacle 542 pH/conductivity meter, Corning, NY). A sourcemeter (2410 Sourcemeter, Keithley Instruments Inc., Cleveland, OH) supplied power to the pump in galvanostatic mode while simultaneously measuring voltage. A MEMs-based liquid flow sensor (Sensirion, Westlake Village, CA) measured instantaneous flow rates at a frequency of 1 Hz. We measured pressure in the cathode reservoir with a pressure transducer (Omega PX303-015G5 V, Stamford, CT). We adjusted the pressure load on the pump by changing the height of a deionized (DI) water column in a large-diameter reservoir. See supplementary information for a schematic of the experimental setup, further details on pump housing and assembly, and glass substrate porosimetry results.

## 3. Results and discussion

### 3.1. Two-liquid EO pump performance

Fig. 2 presents the transient evolution of maximum flow rate, $Q_{max}$, and applied voltage, $V_{app}$, at eight applied currents, $I$, ranging from 25 to 200 μA. Maximum flow rate refers to flow rate at zero pressure load. Between each experiment, the anode and cathode reservoirs were evacuated with a syringe, the anode reservoir refilled with fresh buffer solution, and the secondary fluid reservoir filled with DI water. These experiments were terminated when the secondary fluid reservoir was completely discharged, which was

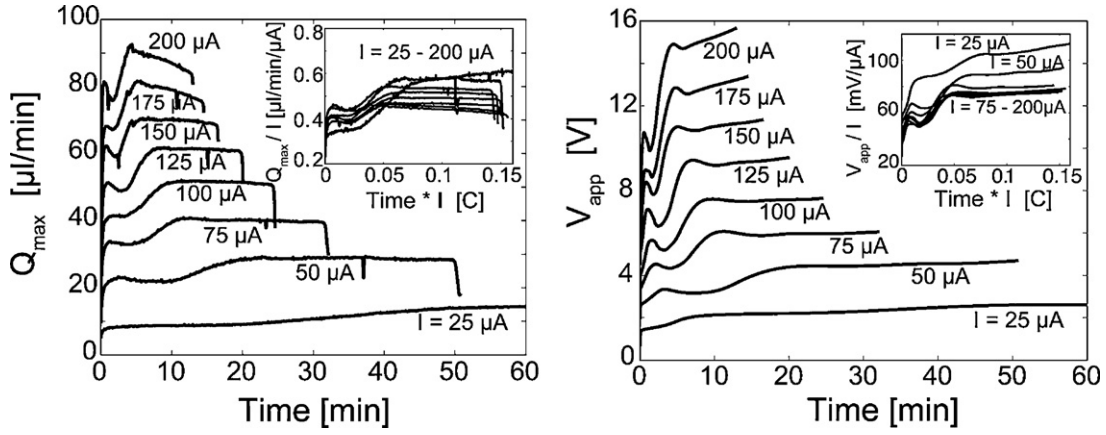


**Fig. 2.** Time-series of (a) maximum flow rate and (b) applied voltage for applied constant currents between 25 and 200 μA. The time series were terminated when the secondary fluid reservoir was discharged. In (a), after an initial transient, an approximately constant pump flow rate was maintained for currents below 175 μA. Inset shows maximum flow rate scaled by applied current versus the product of time and current for all realizations shown in the main figure. The scaling largely collapsed the flow rate transients and magnitude of the curves. In (b), all applied voltages remain under 20 V. Inset shows scaled voltage versus time data, and we again see a fairly good collapse of the curves.

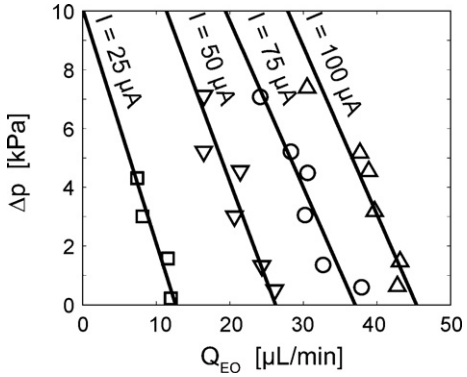


**Fig. 3.** Pump performance curves for the two-liquid EO pump at currents of 25, 50, 75, and 100 μA. Results show that flow rate varies linearly with pressure load for a fixed applied current. The two-liquid, two-membrane pump can generate a flow rate of 13 μl/min against a pressure load of 1.6 kPa while requiring only 25 μA and 73 μW applied power.

evident as a sharp decrease in flow rate (Fig. 2a). After initial start-up transients, stable levels of flow rate and voltage were obtained, except at currents greater than about 175 μA, where we observed gradual decreases in flow rate. In the insets of Fig. 2, we plot $Q_{max}$ and $V_{app}$ divided by applied current, each versus the product of time and current. We discuss these scaled data further in Section 3.2.

We additionally plotted the maximum flow rate and applied voltage versus applied currents ranging from 25 to 200 μA (see Supplementary Information). The flow rate and voltage both exhibit a linear relationship with applied current ($R^2$ = 0.9905 and 0.9989, respectively) as expected. For the lowest applied current of 25 μA, the steady-state voltage is 2.65 V, which generates a flow rate of 14.4 μl/min.

The results presented so far have been for a zero pressure load. However, many applications, such as drug delivery, have a finite pressure load. For example, central vein pressure of approximately 1.4 kPa may serve as an estimated minimum pressure for a drug delivery pump [15]. In Fig. 3, we present data for working flow rate, $Q_{EO}$, against fixed hydrostatic pressure loads, $\Delta p$, between 0 and 8 kPa at currents of 25, 50, 75, and 100 μA. All other experimental details are those of Fig. 2. The flow rate reported here is the mean flow rate for the first 1.0 ml out of the total 1.5 ml pumped from the secondary fluid reservoir. Shown with the data are linear regression fits, which exhibit the expected negative linear slope. The EO pump requires minimal voltage and power. For instance, at 25 μA the EO pump generates 13 μl/min against 1.6 kPa with a voltage of 2.9 V. The calculated thermodynamic efficiency ($Q\Delta p/V_{app}I$) is 0.5% (a typical value for EO pumps [1]), but the pump consumes only 73 μW.

### 3.2. Scaling

Again note the insets of Fig. 2a and b, where we scale flow rate and applied voltage by current and plot these versus the product of time and current. This scaling approximately collapses transients associated with the pump performance. For example, upon application of current, typically voltage and flow rate both increase until roughly 0.01 C of charge is transferred, reaching a temporary plateau value (or local minima), and then increase again until about 0.05 C, at which point a final relatively steady value is reached. We also observe self-similarity in the shape of initial transients, the flow rate and voltage magnitudes of the approximately constant flow region, and the time to full discharge. This scaling shows the importance of the coupling between electromigration (namely, total transferred electrical charge) and bulk flow in this device.

Recent visualizations by Strickland et al. [16] showed that propagating concentration polarization (CP) occurs in porous glass EO pump systems with order 100 nm pore diameter. CP develops in systems where EDL counter ions (counter to wall charge) carry a significant portion of the total ionic current, resulting in enrichment and depletion of ionic strength at the outlet and inlet, respectively, of electrokinetic nanochannels and nanopores [17–19]. For our experimental conditions, we calculate a Dukhin number (ratio of EDL conductivity to bulk conductivity [20]) of approximately 1 using our pump's mean pore radius as a characteristic length scale. We thus hypothesize that the initial transients shown in Fig. 2 are a result of the effect of CP on system spatiotemporal ionic strength. This hypothesis is further reinforced by the highly correlated initial transients in $V_{app}/I$ and $Q_{max}/I$. As discussed by Yao and Santiago [2], EO pump flow rate per current scales as the ratio of zeta potential to working solution conductivity, and zeta potential increases with decreasing conductivity. Therefore, the increase in $Q_{max}/I$ and correlated increase in $V_{app}/I$ are likely attributable to a decrease in bulk conductivity inside the pump pores. Analytical and numerical models presented by Mani et al. [17] and Zangle et al. [18] predict a similar phenomena (decreasing ionic strength) within the nanochannel of serial micro–nano-microchannel systems with surface conductivity on the order of bulk conductivity.

Lastly, we comment on the issue of electrolysis gas bubbles. During pump operations, for all data shown here, we did not observe visible gas bubble formation at system electrodes. We suspect that the solubility of the oxygen and hydrogen in the buffer solution mitigated the effects of gas evolution.

## 4. Conclusion

We presented the performance of a two-liquid EO pump which uses an impermeable, collapsible membrane to separate the fluid delivered by the system from an electrolyte solution optimized for EO pumping. Using a porous glass structure with a 225 nm median pore radius, we achieved pumping against pressure loads consistent with drug delivery using relatively low voltages. For instance, at 25 μA the pump generated a flow rate of 13 μl/min against 1.6 kPa, while requiring an applied voltage of 2.9 V and power of 73 μW. We observed negligible effects of electrolysis bubbles on device performance.

We found both the magnitude and timing of transients in both pump flow rate and applied voltage collapse when scaled by applied current and plotted versus total charge transferred (in Coulombs). This scaling shows the importance of the coupling of charge and mass transfer. Also, this scaling and the characteristic Dukhin number of the system (which was order unity) led us to hypothesize that concentration polarization plays an important rule in the performance of our pump. We hope to study and leverage these effects further.

## Acknowledgments

The authors gratefully acknowledge support from the Department of Defense under contract number W81XWH-07-1-0384. SL and MES were supported by post-graduate scholarships from the Natural Sciences and Engineering Research Council (NSERC) of Canada. The authors also acknowledge the support of EoPlex Technologies in supplying the porous glass samples and the pore size distribution data.

## Appendix A. Supplementary data

Supplementary data associated with this article can be found, in the online version, at doi:10.1016/j.sna.2010.07.008.

## References


[1] D.J. Laser, J.G. Santiago, A review of micropumps, J. Micromech. Microeng. 14 (2004) R35–R64.
[2] S.H. Yao, J.G. Santiago, Porous glass electroosmotic pumps: theory, J. Colloid Interface Sci. 268 (2003) 133–142.
[3] S.H. Yao, D.E. Hertzog, S.L. Zeng, J.C. Mikkelsen, J.G. Santiago, Porous glass electroosmotic pumps: design and experiments, J. Colloid Interface Sci. 268 (2003) 143–153.
[4] S. Zeng, C.-H. Chen, J.C. Mikkelsen, J.G. Santiago, Fabrication and characterization of electroosmotic micropumps, Sens. Actuators B 79 (2001) 107–114.
[5] C.H. Chen, J.G. Santiago, A planar electroosmotic micropump, J. Microelectromech. Syst. 11 (2002) 672–683.
[6] P. Wang, Z.L. Chen, H.C. Chang, A new electro-osmotic pump based on silica monoliths, Sens. Actuators B 113 (2006) 500–509.
[7] Y. Takemori, S. Horiike, T. Nishimoto, H. Nakanishi, T. Yoshida, High pressure electroosmotic pump packed with uniform silica nanospheres, 13th Int. Conf. Solid-State Sens. Actuators Microsyst. 2 (2005) 1573–1576.
[8] A. Nisar, N. Afzulpurkar, B. Mahaisavariya, A. Tuantranont, MEMS-based micropumps in drug delivery and biomedical applications, Sens. Actuators B 130 (2008) 917–942.
[9] A. Brask, G. Goranovic, H. Bruus, Theoretical analysis of the low-voltage cascade electro-osmotic pump, Sens. Actuators B 92 (2003) 127–132.
[10] T. Glawdel, C. Elbuken, L.E.J. Lee, C.L. Ren, Microfluidic system with integrated electroosmotic pumps, concentration gradient generator and fish cell line (RTgill-W1)-towards water toxicity testing, Lab Chip 9 (2009) 3243–3250.
[11] A. Brask, G. Goranovic, M.J. Jensen, H. Bruus, A novel electro-osmotic pump design for nonconducting liquids: theoretical analysis of flow rate-pressure characteristics and stability, J. Micromech. Microeng. 15 (2005) 883–891.
[12] E.L.P. Uhlig, W.F. Graydon, W. Zingg, The electro-osmotic actuation of implantable insulin micropumps, J. Biomed. Mater. Res. 17 (1983) 931–943.
[13] D. Kim, C. Buie, J.G. Santiago, Toward electroosmotic flow-driven air pumps for miniaturized PEM fuel cells, ECS Trans. 3 (2006) 1181–1186.
[14] S. Litster, B. Ha, D. Kim, J.G. Santiago, A two-liquid electroosmotic pump for portable drug delivery systems, in: Proceedings of IMECE, November 11–15, Seattle, USA, 2007.
[15] M. Weiss, M. Hug, T. Neff, J. Fischer, Syringe size and flow rate affect drug delivery from syringe pumps, Can. J. Anesth. 47 (2000) 1031–1035.
[16] D.G. Strickland, M.E. Suss, T.A. Zangle, J.G. Santiago, Evidence shows concentration polarization and its propagation can be key factors determining electroosmotic pump performance, Sens. Actuators B 143 (2009) 795–798.
[17] A. Mani, T.A. Zangle, J.G. Santiago, On the propagation of concentration polarization from microchannel–nanochannel interfaces. Part I: Analytical model and characteristic analysis, Langmuir 25 (2009) 3898–3908.
[18] T.A. Zangle, A. Mani, J.G. Santiago, On the propagation of concentration polarization from microchannel–nanochannel interfaces. Part II: Numerical and experimental study, Langmuir 25 (2009) 3909–3916.
[19] S. Ehlert, D. Hlushkou, U. Tallarek, Electrohydrodynamics around single ion-permselective glass beads fixed in a microfluidic device, Microfluid. Nanofluid. 4 (2009) 471–487.
[20] J.J. Lyklema, A. de Keizer, B.H. Bijsterbosch, G.J. Fleer, M.A. Cohen Stuart IV, Electrokinetics and related phenomena, in: Fundamentals of Interface and Colloid Science, Academic Press, 1995, pp. 1-135.


## Biographies

**Shawn Litster** is an Assistant Professor in the Department of Mechanical Engineering at Carnegie Mellon University. He received his Ph.D. in mechanical engineering from Stanford University and his B.Eng. and M.A.Sc. degrees from the University of Victoria. His research focus is micro- and nano-scale transport phenomena in energy conversion technologies where electrochemistry and electrokinetic effects are dominant, including fuel cells and batteries. He has over 28 peer-reviewed publications, including 14 journal articles and two book chapters, as well as three pending patents. He has received best paper awards at meetings of the *Electrochemical Society and American Society of Mechanical Engineers*.

**Matthew E. Suss** received his B.Eng. degree from McGill University, Montreal, in 2007, and M.Sc. at Stanford University, Stanford, CA in 2009. He is currently beginning a Ph.D. at Stanford where his research is supported by an NSERC scholarship from the Canadian government. His work in the Stanford Microfluidics Laboratory focuses on the development of highly efficient electroosmotic micropumps for drug delivery applications.

**Juan G. Santiago** is Associate Professor of Mechanical Engineering at Stanford University and Chair of the Thermosciences Group. He specializes in microscale transport phenomena and electrokinetics. He earned his Ph.D. in Mechanical Engineering from the University of Illinois at Urbana-Champaign. Among other awards, he won the National Science Foundation Presidential Early Career Award for Scientists and Engineers (PECASE) ('03–'08). Santiago has presented 13 keynote and named lectures and over 100 additional invited lectures. His group has been awarded ten best paper and poster awards. He has authored/co-authored over 110 archival publications, authored/co-authored 200 conference papers, and holds 25 patents.